

Crossover from Hydrodynamics to the Kinetic Regime in Confined Nanoflows

C. Lissandrello, V. Yakhot, and K. L. Ekinci

Department of Mechanical Engineering, Boston University, Boston, Massachusetts 02215, USA

(Dated: December 3, 2024)

We present an experimental study of a confined nanoflow, which is generated by a sphere oscillating in the proximity of a flat solid wall in a simple fluid. Varying the oscillation frequency, the confining length scale and the fluid mean free path over a broad range provides a detailed map of the flow. We use this experimental map to construct a scaling function, which seamlessly describes the nanoflow in the entire parameter space, including both the hydrodynamic and the kinetic regimes. Our scaling function unifies previous theories based on the slip boundary condition and the effective viscosity.

In micron and nanometer scale flows [1, 2], the characteristic dynamic length scale \mathcal{L} of the flow approaches and is even exceeded by the mean free path of the fluid λ . This limit is clearly beyond the applicability of the Navier-Stokes equations, requiring a rigorous treatment using kinetic theory. A less rigorous but widely used approach to describe these small scale flows is to extend the Newtonian description by imposing a slip boundary condition on solid walls. This approach is justified as follows. Derivation of the Navier-Stokes equations from kinetic theory results in the appearance of a Knudsen layer of thickness λ near the wall [3]. Because a fluid element of linear dimension $\sim \lambda$ is treated as a mathematical point in the hydrodynamic approximation, the velocity at the wall becomes $u_w \approx \lambda \frac{du}{dz}|_{z=0}$, with u being the hydrodynamic velocity (assumed parallel to the wall) and $\hat{\mathbf{z}}$ being the wall normal. Thus, the slip length b , where $b \sim \lambda$, is applied as a convenient empirical parameter to extend the Navier-Stokes equations into the kinetic regime. As required by macroscopic hydrodynamics, b becomes negligible when the Knudsen number, $\text{Kn} \equiv \frac{\lambda}{\mathcal{L}}$, is small, i.e., $\text{Kn} \ll 1$.

The above approach comes with some problems. To describe some gas flows, for instance, unphysical slip lengths, $b \gg \lambda$, may be required. To alleviate this problem, one can assume specular reflections of the gas molecules from the wall. Yet, experiments show that this assumption is not very accurate for heavier gases and untreated surfaces [4, 5]. Worse is the problem when the Navier-Stokes solution (with the slip boundary condition) fails to converge with the prediction of the kinetic theory. A good example to the point is oscillating nanoflows [6–8]. Efforts to describe oscillating nanoflows using the Navier-Stokes equations in conjunction with a slip length agree with experiments only in a range of relevant parameters [9]. A proper kinetic treatment of the problem [10] shows why: the finite relaxation time τ of the fluid modifies the physics of the flow, resulting in the “telegrapher’s equation”, which is substantially different from the Navier-Stokes equations.

In this manuscript, we turn our attention to nanometer scale confined flows in the limit $h \lesssim \lambda$, where h is the confining length scale. So far, a group of researchers have extended Reynolds’ hydrodynamic formulation [11, 12]

to small scales by imposing the slip boundary condition [13–17] — as described above. Others, coming from kinetic theory, have developed the concept of the effective viscosity, which typically depends upon a properly defined Knudsen number [18, 19]. There is no question that both approaches must agree for the same flow parameter space. Here, we present an experimental study of nanometer scale confined flows covering a broad range of parameters — including gap h , pressure p , and frequency $\frac{\omega}{2\pi}$ — along with a scaling theory. Our scaling function describes the physical behavior of the flow in the entire parameter space, capturing the transition from hydrodynamics to the kinetic regime accurately.

We study the oscillatory hydrodynamic response of a sphere in the proximity to a solid surface. Our experimental device is a micron-scale silica sphere with radius R glued to the end of a microcantilever of linear dimensions $l \times w \times t$. We have employed both the fundamental and first harmonic flexural modes of a soft cantilever (C1), and the fundamental flexural mode of a shorter stiffer cantilever (C2). Figure 1(a) depicts optical measurements and simulations (inset) of the mechanical modes of C1. For each device and mode, we first extract the the intrinsic quality factor Q_i and resonance frequency $\frac{\omega_i}{2\pi}$ in UHV away from any surfaces. The modal mass m_e is determined from the resonance frequency shifts before and after the sphere is attached to the cantilever. These parameters are listed in Table I.

Once the mechanical mode is characterized, we change the flow parameters while optically monitoring the dissipation and the resonance frequency of the mode. In particular, we continuously vary two parameters for each mode: i) we change the gap h (shortest distance) between the sphere and a flat solid (Silicon) surface using a calibrated positioner; ii) we vary the surrounding pressure p by admitting dry N_2 into the chamber. This provides a two-dimensional parametric map of the dimensionless dissipation and the (angular) resonance frequency: $Q_m^{-1} = Q_m^{-1}(h, p)$ and $\omega_m = \omega_m(h, p)$. Before presenting the data, we show in Fig. 1(b) that $1/Q_m$ measured by linearly driving the resonator and by monitoring its thermal fluctuations agree closely, with a typical discrepancy less than 1%. By properly subtracting the intrinsic dissipation from the measured dissipation, one

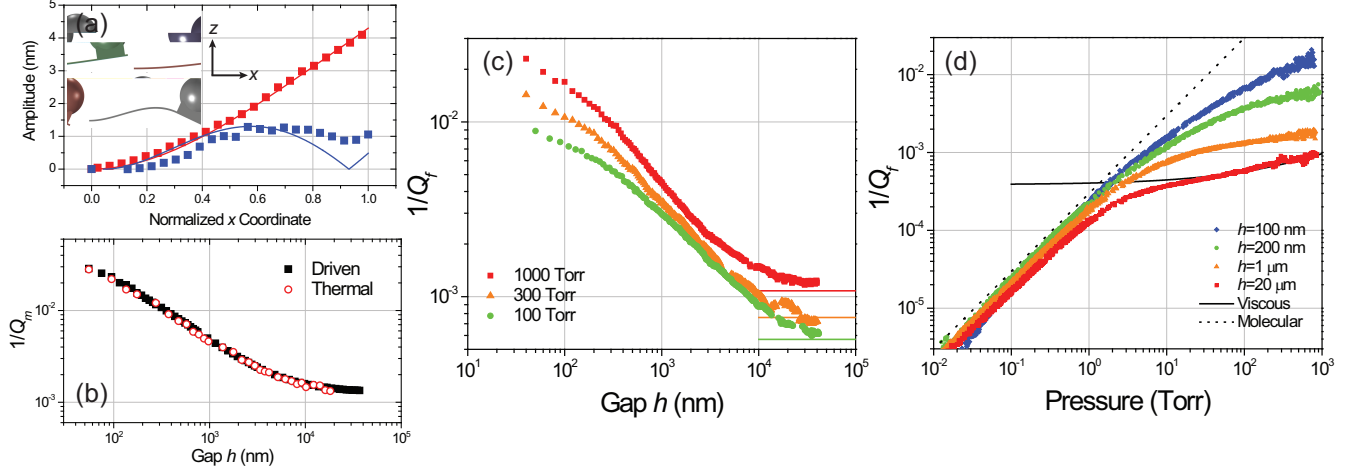


FIG. 1. (a) Measured and simulated (inset) mechanical modeshapes of the sphere-cantilever device (C1). The solid lines are fits using simple beam theory. In the first harmonic mode, the node appears at the position where the sphere is attached. (b) Measured dimensionless dissipation $1/Q_m$ as a function of gap h , using two different techniques. First, Q_m is obtained from a fit to the driven frequency response of the device. Second, Q_m is extracted from a fit to the power spectral density of the thermal oscillations of the device. (c) Dimensionless fluidic dissipation $1/Q_f$ measured as a function of gap h at fixed pressures p . Solid line segments come from viscous theory given by Eq. (1) and Ref. [21]. (d) $1/Q_f$ measured as a function of pressure p with the gap fixed. Solid line is from viscous theory as in (c). The dotted line is from molecular theory [9]. All data in this figure are obtained from device C1.

can obtain the fluidic dissipation: $1/Q_f = 1/Q_m - 1/Q_i$. Figure 1(c) and (d) show the $Q_f^{-1} = Q_f^{-1}(h, p)$ data set for the 13.7 kHz mode, plotted against the pressure p and gap h axes, respectively. In Fig. 1(c), the gap is varied in the range $10^{-8} \text{ m} \leq h \leq 10^{-4} \text{ m}$ with the pressure held at $p = 100, 300$ and 1000 Torr. Conversely, in Fig. 1(d), the pressure is swept continuously in the range $10^{-2} \text{ Torr} \leq p \leq 10^3 \text{ Torr}$, while the gap is fixed at $h = 0.1, 0.2, 1$ and $20 \mu\text{m}$. The accompanying mode frequency data, $\omega_m = \omega_m(h, p)$, show very little variation (less than 0.1%) in this parameter space and will not be taken into account in this work.

Several important preliminary observations can be made from the data of Fig. 1(c) and (d). For a sphere oscillating at frequency $\frac{\omega}{2\pi}$ in an unbounded fluid at the viscous limit $\omega\tau \ll 1$ [6, 10], the dimensionless dissipation can be written as [20]

$$\frac{1}{Q_{f\infty}} = \frac{6\pi\mu R}{m\omega} \left(1 + \frac{R}{\delta}\right), \quad (1)$$

where R is the radius and m is the mass of the sphere, μ is the dynamic viscosity of the fluid, and $\delta = \sqrt{\frac{2\mu}{\rho\omega}}$ is the viscous boundary layer thickness. As usual, $\mu = \rho\nu$, where ρ is the density and ν is the kinematic viscosity of the fluid. The fluidic dissipation from the rectangular cantilever can also be found, albeit numerically [21]. The solid line segments in Fig. 1(c) and solid curve in Fig. 1(d) show the $1/Q_{f\infty}$ predictions of viscous theory using the parameters of our experimental system at large gaps, $h \rightarrow \infty$. In Fig. 1 (d), the prediction of molecular

TABLE I. Mechanical properties of the measured devices.

Device	Mode	$l \times w \times t$ (μm)	R (μm)	$\frac{\omega_i}{2\pi}$ (kHz)	Q_i	m_e (kg)
C1	1	$230 \times 40 \times 3$	35	13.7	12×10^3	5×10^{-10}
C1	2	$230 \times 40 \times 3$	35	45.8	3.4×10^3	16×10^{-10}
C2	1	$125 \times 35 \times 4$	21.5	122.4	6.8×10^3	1×10^{-10}

theory [9] is also shown at low pressure. The close agreement of the data with theory at the proper limits gives us confidence to move forward.

Though it is clear that the entire velocity field is substantially modified by the presence of the stationary wall, the dissipation caused by the squeezing of fluid in the gap can be conveniently studied by subtracting the dissipation in an infinite fluid, i.e., $1/Q_h = 1/Q_f - 1/Q_{f\infty}$. Experimentally, $1/Q_{f\infty}$ can be found from the flat h -independent asymptotes in Fig. 1(c). Subtracting these asymptotic values results in the gap-dependent dimensionless dissipation $1/Q_h$.

Figure 2 depicts $1/Q_h$ measured for three different modes at multiple pressures as the gap is varied. Solid lines are fits to theory, which will be discussed below. A first pass analysis of the data can be provided based upon the dimensionless Knudsen number, $\text{Kn}_h \equiv \frac{\lambda}{h}$. When $\text{Kn}_h \ll 1$, $1/Q_h \propto 1/h$, which is the familiar hydrodynamic lubrication result [22–24]:

$$\frac{1}{Q_h} = \frac{6\pi\mu R}{m\omega} \times \frac{R}{h}. \quad (2)$$

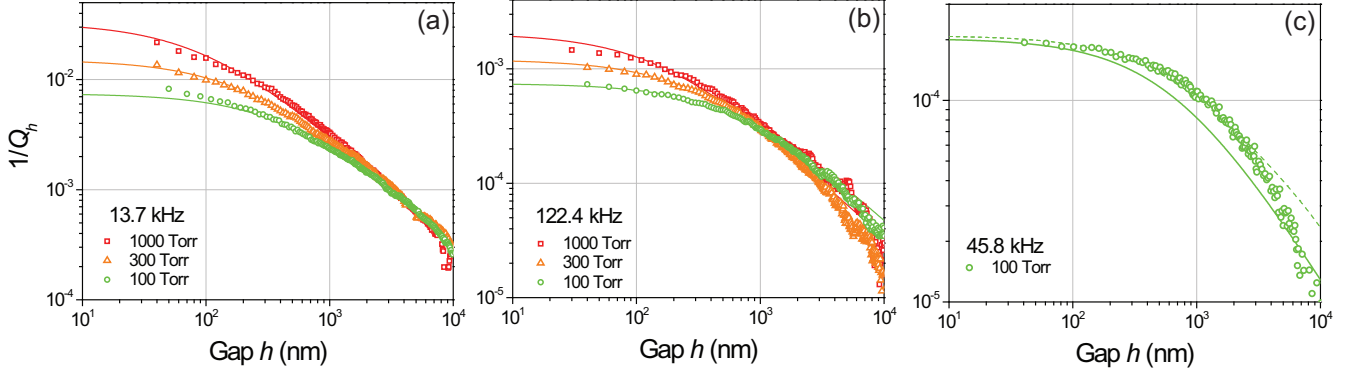


FIG. 2. Gap dependent dimensionless dissipation $1/Q_h$ as a function of gap h at fixed pressure. Solid lines are fits to Eq. (7) with $\alpha = 0.5$ and $\beta = 1.6$. Data in (a) and (b) are from the fundamental modes of devices C1 and C2. (c) Data from the first harmonic mode of device C1. The slight deviation from the solid line is possibly due to the additional rotational motion of the sphere. The dashed line is the improved fit with the added rotational dissipation [22]. To improve the fits, theoretical curves have been divided by fitting factors of 4 ± 1 .

At the opposite limit, the dimensionless dissipation saturates. Between these two limits, there is a well-defined transition from the hydrodynamic to the kinetic regime.

We now provide a theoretical background for the observed transition. Since $1/Q_h \rightarrow 0$ as $h \rightarrow \infty$, we can write a general relation

$$\frac{1}{Q_h} = \frac{6\pi\mu R}{m\omega} \times \frac{R}{h} \times f\left(\frac{\lambda}{h}, \frac{\lambda}{\delta}, \frac{\lambda}{R}, \dots, \frac{R}{\delta}\right). \quad (3)$$

The scaling function $f(\{x_i\})$, which is analytic in the limit $\{x_i\} \rightarrow 0$, depends on various dimensionless variables pertaining to different dynamic regimes. It is clear that the first few $\{x_i\}$ are the familiar Knudsen numbers based on appropriate linear dimensions characterizing the system: $\text{Kn}_h = \frac{\lambda}{h}$, $\text{Kn}_\delta = \frac{\lambda}{\delta}$, $\text{Kn}_R = \frac{\lambda}{R}$ and so on.

The last dimensionless variable, $\frac{R}{\delta} = R\sqrt{\frac{\omega}{2\nu}} = \sqrt{\frac{UR}{\nu}} = \text{Re}_\delta$, can be regarded as a Reynolds number based on the velocity $U = \omega R/2$. In the limit $\text{Kn}_i \rightarrow 0$ and $\text{Re}_\delta \rightarrow 0$, Taylor expansion gives

$$\frac{1}{Q_h} = \frac{6\pi\mu R}{m\omega} \times \frac{R}{h} \times \left(1 + f^{(1)} + f^{(2)} + \dots\right) \quad (4)$$

where

$$f^{(1)} = a_h^{(1)} \text{Kn}_h + a_\delta^{(1)} \text{Kn}_\delta + \dots + a_{\text{Re}}^{(1)} \text{Re}_\delta \quad (5)$$

$$f^{(2)} = a_h^{(2)} \text{Kn}_h^2 + a_\delta^{(2)} \text{Kn}_\delta^2 + \dots + a_{\text{Re}}^{(2)} \text{Re}_\delta^2 + a_{h,\delta}^{(2)} \text{Kn}_h \text{Kn}_\delta + a_{h,\text{Re}}^{(2)} \text{Kn}_h \text{Re}_\delta + \dots \quad (6)$$

The relative magnitudes of the $a_i^{(n)}$ and the dimensionless parameters $\{x_i\}$ will determine the physics of the flow. By varying $\{x_i\}$ over a broad range, one can extract the magnitudes of $a_i^{(n)}$ from experiment. This is indeed what we have done.

To gain more insight into the proposed expansion in Eq. (4), let us consider the limits. When $h \rightarrow \infty$ ($\text{Kn}_h \rightarrow 0$), experimental dimensionless dissipation due to squeezing disappears, $1/Q_h \rightarrow 0$. This suggests that the first order term in the Taylor expansion in Eq. (5) should not strongly depend on the other Knudsen numbers, Kn_δ , Kn_R and so on. In the limit of small h ($\text{Kn}_h \gg 1$), momentum transfer is dominated by the ballistic impact of the molecules emitted from the stationary plate incident on the moving sphere. The contribution of intermolecular collisions can be neglected. If the thermal molecular velocity u_{th} is large, the dimension of the gap h must disappear from the expression for dissipation. A possible expression, which is a consequence of Eqs. (4-6) and leads to expected behavior in both physical limits, can be written as

$$\frac{1}{Q_h} = \frac{6\pi\mu R}{m\omega} \times \frac{R}{h} \times \frac{1}{1 + \alpha \frac{\lambda}{h} (1 + \beta \frac{R}{\delta})}. \quad (7)$$

This expression can be perceived as the simplest Padé approximant, which agrees with the experiments. The constants α and β are related to $a_i^{(n)}$. It is interesting to note that, in this choice, the term of linear order $\mathcal{O}(\text{Re}_\delta)$ disappears due to the subtraction, $1/Q_h = 1/Q_f - 1/Q_{f\infty}$. However, the higher order term $\mathcal{O}(\text{Kn}_h \text{Re}_\delta)$ survives. In the small-gap limit $\text{Kn}_h = \frac{\lambda}{h} \gg 1$, one obtains as prescribed

$$\frac{1}{Q_h} \approx \frac{6\pi\rho u_{th} R^2}{m\omega\alpha (1 + \beta \frac{R}{\delta})}. \quad (8)$$

Returning to Fig. 2, we now describe how the fits to the experimental data are obtained based upon the above scaling form. The device parameters $m = m_e$, ω , and R are experimental constants. The fluid parameters are all assumed to be independent of h , but may depend on p :

$\lambda \propto p^{-1}$, $\delta \propto p^{-1/2}$, and μ is independent of p . The very *same* constants α and β in the scaling function of Eq. (7) must uniquely fit *all* data sets — regardless of pressure, frequency, mode and so on. Indeed, we can fit *all* our data with $\alpha = 0.5$ and $\beta = 1.6$. We emphasize that any small changes in α and β cause the curves in Fig. 2 to shift along the h -axis, making the fits unacceptable. While α and β determine the shape of the curves uniquely, the fits can be improved along the $1/Q_h$ -axis by dividing the theoretical curves by fitting factors of order ~ 4 . The results of this exercise are the solid curves in Fig. 2(a)-(c). We estimate that these fitting factors may be needed because i) the sphere is not ideal in shape (due to the cantilever and epoxy above it), ii) m_e is hard to determine, especially for the first harmonic mode, and iii) the sphere oscillations are not absolutely normal to the wall (see further discussion below).

The above-described fit in Fig. 2(c) (solid curve) deviates slightly from the data for $10^2 \text{ nm} \lesssim h \lesssim 5 \times 10^4 \text{ nm}$. Here, finite element simulations suggest that the sphere undergoes rotational motion in addition to its normal oscillations, with $\omega R \sim 4 |\dot{h}|$, where $|\dot{h}|$ is the magnitude of the oscillation velocity of the sphere normal to the wall. Pure rotational motion results in a dimensionless dissipation with a different functional form, $1/Q_h \propto \ln h$, due to shearing of the fluid [22]. One could incorporate this motion into the fits by adding a $\ln h$ term to the $1/h$ term in Eq. (3), but keeping the scaling function exactly the same. The dashed line in Fig. 2(c) is this improved fit. To obtain the fit, we have weighted the rotational dissipation and the dissipation due to squeezing based on finite element simulation results. However, the effect remains small, suggesting that $\sim 1/h$ dependence can be assumed prevalent for all devices considered here and in the literature.

Having fit individual data traces, we can collapse all our data as shown in Fig. 3. The collapse is obtained by removing the trivial effects of the device size and frequency from the data as well as the more profound effects of the scaling function $f(\{x_i\})$. The plotted dimensionless quantity, $\frac{1}{Q_h} \times \frac{m\omega}{6\pi\mu R} \times \frac{1}{f}$ can be regarded as the dimensionless size- and frequency-independent dissipation, in which the kinetic effects have been deconvoluted. It therefore shows the hydrodynamic R/h dependence at all length scales studied here.

Finally, our results can be interpreted as follows. In the hydrodynamic limit ($h \gg \lambda$), this problem is described by Eq. (2), where the viscosity μ is dominated by intermolecular collisions, $\mu \sim \rho u_{th} \lambda$, with a relaxation time-scale $\sim \lambda/u_{th}$. To gain insight into the kinetic limit ($h \ll \lambda$), one can simply write the shear stress on the sphere as $\sigma \sim \rho u_{th} |\dot{h}|$. It is easy to see that $\sigma \sim \rho u_{th} h \frac{|\dot{h}|}{h} \sim \rho u_{th} h \frac{du}{dz}$, where $\frac{du}{dz}$ is the velocity gradient. This result can be interpreted as the appearance of

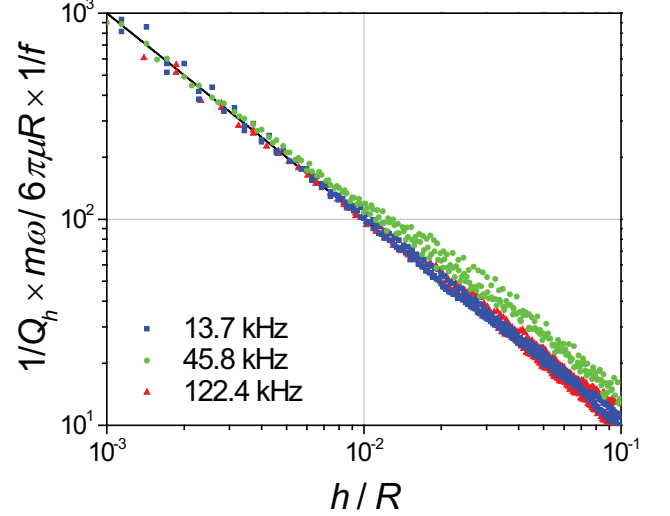


FIG. 3. Collapse of all experimental data from this work.

an effective viscosity, $\mu_{eff} \approx \rho u_{th} h$, due to an effective mean free path, $\lambda_{eff} \approx h$. Substituting μ_{eff} into the hydrodynamic solution simply results in $\frac{1}{Q_h} \sim \frac{6\pi\rho u_{th} R^2}{m\omega}$, consistent with Eq. (8). Thus, in principle, one may justify an attempt to reach the kinetic regime by using the Navier-Stokes equations, but combined with effective (and sometimes frequency-dependent) viscosities, slip lengths and so on. In this manuscript, we have presented experimental data on confined nanoflows covering a broad range of flow parameters, and developed a simple scaling theory to describe experiments in the entire parameter range — without explicitly employing an effective viscosity and slip length. To conclude, we stress that the dimensionless Weissenberg number here remains small, $Wi = \omega\tau \ll 1$. Since the appearance of frequency in effective viscosity essentially leads to a modification of the equations of motion [6, 10], generalization of confined nanoflows to the interval $Wi \gg 1$ will require further experimental and theoretical work.

The authors acknowledge generous support from the US NSF (through grants DGE-0741448, ECCS-0643178 and CMMI-0970071).

-
- [1] G. Karniadakis, A. Beskok, and N. Aluru, *Microflows and Nanoflows* (Springer, New York, 2005).
 - [2] P. Tabeling, *Introduction to Microfluidics* (Oxford, New York, 2005).
 - [3] E. M. Lifshitz and L. P. Pitaevskii, *Physical Kinetics* (Butterworth-Heinemann, Oxford, 1981).
 - [4] E. B. Arkilic, K. S. Breuer, and M. A. Schmidt, *J. Fluid Mech.* **437**, 29 (2001).
 - [5] W. M. Trott, J. N. Castaeda, J. R. Torczynski, M. A. Gallis, and D. J. Rader, *Rev. Sci. Instrum.* **82**, 035120

- (2011).
- [6] D. M. Karabacak, V. Yakhot, and K. L. Ekinici, Phys. Rev. Lett. **98**, 254505 (2007); K. L. Ekinici, D. M. Karabacak, and V. Yakhot, Phys. Rev. Lett. **101**, 264501 (2008); K. L. Ekinici, V. Yakhot, S. Rajauria, C. Colosqui, and D. M. Karabacak, Lab Chip **10**, 3013 (2010).
 - [7] O. Svitelskiy, V. Sauer, N. Liu, K.-M. Cheng, E. Finley, M. R. Freeman, and W. K. Hiebert, Phys. Rev. Lett. **103**, 244501 (2009).
 - [8] E. J. Lee, C. S. Kim, Y. D. Park, T. Kouh, J. Nanosci. Nanotechnol. **11**, 6599 (2011).
 - [9] R. B. Bhiladvala and Z. J. Wang, Phys. Rev. E **69**, 036307 (2004).
 - [10] V. Yakhot and C. Colosqui, J. Fluid Mech. **586**, 249 (2007).
 - [11] O. Reynolds, Philos. Trans. R. Soc. London **177**, 157 (1886).
 - [12] O. I. Vinogradova, Langmuir **11**, 2213 (1995).
 - [13] A. Maali and B. Bhushan, Phys. Rev. E **78**, 027302 (2008).
 - [14] C. D. F. Honig, J. E. Sader, P. Mulvaney, and W. A. Ducker, Phys. Rev. E **81**, 056305 (2010).
 - [15] A. P. Bowles and W. A. Ducker, Phys. Rev. E **83**, 056328 (2011).
 - [16] J. Laurent, A. Drezet, H. Sellier, J. Chevrier, and S. Huant, Phys. Rev. Lett. **107**, 164501 (2011).
 - [17] S. Ramanathan, D. L. Koch, and R. B. Bhiladvala, Phys. Fluids **22**, 103101 (2010).
 - [18] M. Bao, H. Yang, H. Yin, and Y. Sun, J. Micromech. Microeng. **12**, 341 (2002).
 - [19] T. Veijola, H. Kuisma, and J. Lahdenper, Sens. Actuators, A **66**, 83 (1998).
 - [20] L. D. Landau and E. M. Lifshitz, *Fluid Mechanics*, 2nd ed. (Butterworth-Heinemann, Oxford, 1987).
 - [21] J. E. Sader, J. W. M. Chon, and P. Mulvaney, Rev. Sci. Instrum. **70**, 3967 (1999).
 - [22] S. Kim and S. J. Karrila, *Microhydrodynamics* (Butterworth-Heinemann, Boston, 1991).
 - [23] R. S. Chadwick and Z. Liao, SIAM Soc Ind Appl Math. **50**, 313 (2008).
 - [24] H. Brenner, Chem. Eng. Sci. **16**, 242 (1961).